K^+N phase shifts from 600 to 1500 MeV/c

Keiji Hashimoto
Department of Physics, Virginia Polytechnic Institute and State University, Blacksburg, Virginia 24061
and Department of Nuclear Engineering, Kyoto University, Kyoto 606, Japan
(Received 21 November 1983)

K^+-nucleon phase shifts are presented in the region 600—1500 MeV/c laboratory kaon momentum. They are obtained by a single-energy phase-shift analysis for the KN $I=1$ and $I=0$ states using world data including recently measured $P(K^+n\rightarrow K^+n)$ and $P(K^+n\rightarrow K^0p)$. The result supports the resonances in the P_{13} and D_{03} waves. Other resonancelike structures have also been found in the P_{11} and D_{05} states, which could be interpreted as new candidates for Z^* resonances. In this paper numerical phase shifts are demonstrated as well as their accuracy. These values could be used for future studies on kaon-induced nuclear reactions.

I. INTRODUCTION

A contemporary belief in particle physics is that hadrons are composed of quarks.[1] Low-lying states of hadrons are considered to have the quark configurations qqq and $q\bar{q}$. Most observed hadron states can be assigned to representations of a unitary symmetry generated by quarks. The additional degree of freedom of color has been introduced to retain the Pauli principle in quark systems and to ensure the nonexistence of an isolated single quark state. By assuming that quark configurations are allowed only to be singlets of the color SU(3) group (colorless) and that nature is color blind, it is naturally understood that q^3 and $q\bar{q}$ are the simplest observable configurations.

A color singlet state can be constructed also by more than three quarks and antiquarks such as $q^2\bar{q}^2$, $q^4\bar{q}$, and q^6. The possible existence of such multiquark (exotic) states has been investigated, with considerable effort, in scattering experiments and analyses in the intermediate energy region. Theoretical models have been proposed based on a hadron picture as an extended object, for example, the MIT bag model.[2] In this model the multiquark hadrons can be discussed on, at least qualitatively, the same basis as ordinary hadrons.[3,4]

The K^+N (Z^*) system is a candidate for multiquark states since a three-quark system cannot construct states of hypercharge 2. A possible exotic resonance in the Z^* channel can be understood only by the configuration $q^4\bar{q}$ rather than q^3 with orbital excitations.

A search for the Z^* resonances has been made since the early 1960's. For the KN $I=1$ system the phenomenological understanding has been improved based on relatively rich experiments of K^+p scattering. Our knowledge of the KN $I=0$ state, on the contrary, is far from a comparable quantitative stage owing to experimental difficulties. Although some candidates for the Z^* resonances have been reported based on experimental suggestions and analyses, the existence of the resonances seems to be inconclusive.

Apart from the exotic resonances, there is another interest in studying the KN interaction at low energies. Experimental research on kaon-induced nuclear reactions will be active as a new direction of nuclear structure physics.[5] Also, prospective "kaon factories" will make a great contribution to this field. In this sense it would be necessary to study the "elementary" KN interaction in terms of current experiments and to provide a basis for future developments in kaon nuclear physics.

In this paper a single energy phase-shift analysis is presented which is performed for the KN $I=1$ and $I=0$ states simultaneously. Some recent analyses have employed a parametrization of amplitudes in terms of energy. A motivation of the present analysis was to eliminate possible prejudices owing to a particular functional form of the amplitude and to determine it in a model independent way.

Another motivation of the present analysis was due to new data of $P(K^+n\rightarrow K^+n)$ and $P(K^+n\rightarrow K^0p)$ measured at Rutherford Laboratory and KEK National Laboratory for High Energy Physics.[6] These are the first polarization data for the $I=0$ system in the resonance region. Since the polarization parameter can provide information on the relative phase of the spin amplitudes, these new data are helpful in resolving ambiguities associated with amplitude analyses, especially for the KN $I=0$ system.

A preliminary result of the analysis has already been reported.[7] The present work is improved from the previous one by the introduction of more realistic formulas for K^+-deuteron breakup reaction cross sections based on the impulse approximation. Also, the data base is thoroughly examined in reference to the consistency between experiments and with unitarity. The result is essentially the same as previously reported; it reinforces old resonant solutions for the P_{13} and D_{03} waves, and suggests structures in the P_{11} and D_{05} states, which could be interpreted as new candidates for Z^* resonances.

In this paper numerical phase shifts are demonstrated at 600, 650, 700, 800, 860, 910, 970, 1080, 1170, 1210, 1300, 1360, 1410, 1450, and 1500 MeV/c as well as their accuracy which reflects the quality of current experiments. These values could be applied to calculations in kaon nuclear physics.

The rest of the paper is organized as follows: Section II

contains discussions of the data base. The employed formulas are briefly reviewed in Sec. III, where the deuteron breakup formulas are given in some detail. An outline of the method of the analysis is shown in Sec. IV. The final results are presented in Sec. V in terms of tables and figures. In Sec. VI we discuss implications for Z^* resonances. Section VII is devoted to conclusions.

II. KN EXPERIMENTAL DATA

The data base used in the analysis is summarized in Tables I and II. The data references 8—14, 16—18, 40—44, 51—53, and 56—58 contain a short form like (71A1). This naming convention is taken after a CERN K^+N data compilation[60] for data up to 1974, and for some new K^+p data we adopt the same naming as in the work of Arndt *et al.*[61]

A. K^+p experiments

The KN $I=1$ state can be studied in K^+p scattering experiments. Available data are the total,[8–13] reaction,[14–20] and differential[21–34] cross sections and polarizations.[35–38] As quasi-experimental data, also available are $\alpha=\mathrm{Re}f(0)/\mathrm{Im}f(0)$, where $f(0)$ is the forward K^+p amplitude, calculated by the forward dispersion relation.[39]

The K^+p differential cross sections[21–34] have been measured in almost the entire angle range. There are some measurements for extremely backward scattering.[25,28] They are, however, inconsistent with other accurate data, most likely owing to the normalization problem. These data were not used in the analysis.

The polarizations are available by virtue of four experiments.[35–38] At some momentum points where the polarization data are absent, data at neighboring momenta were used since there is little momentum dependence in the K^+p polarization.

B. K^+d experiments

The isosinglet state of the KN system can be investigated in K^+n elastic and charge exchange ($K^+n\to K^0p$) scattering. Unlike K^+p scattering, however, the study of the K^+n channel has experimental difficulties since no neutron target is available. Most data containing the $I=0$ part are from deuteron targets.

The $I=0$ total[40–42] and reaction[43,44] cross sections are inferred from those of K^+d scattering. A dispersion analysis by Martin[45] presents the real part of the $I=0$ forward amplitude.

The quasi-K^+n elastic scattering cross sections have been obtained from the reaction $K^+d\to K^+np$.[46–48] The measurements by the BGRT collaboration[46,47] extend from 640 to 1510 MeV/c using a deuteron bubble chamber. Below 1000 MeV/c there is a counter experiment at Rutherford Laboratory.[48] These two types of experiments conflict; the latter data are considerably smaller in forward directions.

In the Rutherford experiment the criterion to distinguish the reactions $K^+d\to K^+n(p)$, $K^+p(n)$, and K^+d is not clear (the particle in parentheses represents a spectator), so that the correction owing to the latter two reactions appears to be ambiguous. In fact, the cross sections for $K^+d\to K^+p(n)$, which are also available in Ref. 48, show discrepancies with available data from hydrogen targets at forward angles. The Rutherford experiment presents the cross sections from unconstrained events ($K^+d\to K^+np$ or d). This analysis uses these data. Although contamination of K^+d coherent scattering may be sizable for small angles, the data are consistent with others within the impulse approximation formalism, which will be discussed later.

The cross sections for charge exchange scattering $K^+n\to K^0p$ have also been inferred from the breakup reaction $K^+d\to K^0pp$.[48–55] The BGRT group[52,53] measured the cross sections at 640 through 1510 MeV/c in a deuteron bubble chamber. Most of the other experiments are bubble chamber experiments,[49–51,54,55] and the only one at Rutherford Laboratory[48] uses counters. The data by these experiments are consistent in the entire momentum range concerned.

There was only one polarization measurement in the KN $I=0$ state at 600 MeV/c (Ref. 50) until 1980. This situation has been greatly improved by recent measurements of the K^+n elastic[56,57] and charge exchange[57,58] polarizations. These data have provided a deeper understanding of the KN $I=0$ state and were of great help in the present analysis.

C. Charge exchange by K_L^0 mesons

To be free from an ambiguity due to the deuteron structure, two experiments have presented the charge exchange cross sections for $K_L^0p\to K^+n$ scattering.[59] They, however, show an obvious discrepancy from the breakup data discussed above. Since the K_L^0 particle has both $S=\pm1$ components, these experiments appear to suffer from the normalization problem owing to the uncertainty of the regeneration probability.[59] In the analysis these data are used assuming the normalization uncertainty of 25%.

III. FORMALISM

A. KN two-body formalism

Since the spin-$\frac{1}{2}$ spin-0 scattering formulas are well known, here we review conventions used in this paper.

The KN amplitude F is related to the pure isospin amplitudes F^I as follows:

$$F(K^+p)=F^1+(\text{Coulomb corrections}) , \tag{1}$$

$$F(K^+n\to K^+n)=\tfrac{1}{2}(F^1+F^0) , \tag{2}$$

and

$$F(K^+n\to K^0p)=\tfrac{1}{2}(F^1-F^0) . \tag{3}$$

The c.m. spin non-flip and flip amplitudes, f and g, are introduced as

$$F^I(\theta)=f^I(\theta)+i\vec{\sigma}\cdot\hat{n}g^I(\theta) , \tag{4}$$

where

$$\hat{n}=\vec{k}\times\vec{k}'/|\vec{k}\times\vec{k}'| . \tag{5}$$

TABLE I. KN forward data.[a]

P_{lab} (MeV/c)	Data	Reference	P_{lab} (MeV/c)	Data	Reference
		σ_{tot} (K^+p) (mb)			
600	12.32 ±0.09	*12* 611	650	12.32 ±0.09	*12* 611
700	12.25 ±0.08	*12* 719	800	12.76 ±0.11	*12* 795
860	13.47 ±0.08	*12* 872	910	14.32 ±0.10	*12* 897,924
970	15.52 ±0.08	*12* 977	1090	17.36 ±0.30	*10* 1094
					13 1090
1170	17.95 ±0.35	*13* 1160	1210	18.58 ±0.90	*10* 1210
1300	18.53 ±0.13	*9* 1293	1360	18.36 ±0.14	*9* 1347
		10 1295			*10* 1345
1410	18.12 ±0.14	*9* 1408	1450	18.04 ±0.10	*10* 1445
		10 1395	1500	17.93 ±0.09	*10* 1495
		σ_r (K^+p) (mb)			
600	0.00 ±0.01		650	0.06 ±0.03	*14* 642
700	0.10 ±0.03	*14* 642	800	0.95 ±0.16	*14* 810
		16 735			
860	1.64 ±0.07	*17* 864	910	2.20 ±0.12	*18* 900
970	4.01 ±0.25	*18* 970	1090	6.45 ±0.31	*18* 1060,1130
1170	7.28 ±0.31	*18* 1130	1210	7.72 ±0.25	*18* 1210
		17 1207			*20* 1210
1300	8.52 ±0.19	*18* 1320	1360	8.45 ±0.19	*18* 1380
		20 1290			*20* 1380
1410	8.45 ±0.19	*18* 1380	1450	8.72 ±0.22	*18* 1480
		20 1380			*15* 1455
1500	8.86 ±0.22	*18* 1480			
		15 1455			
		19 1520			
		α (K^+p)[b]			
600	−1.72 ±0.17	*39* 600	650	−1.56 ±0.17	*39* 600,700
700	−1.41 ±0.14	*39* 700	800	−1.03 ±0.10	*39* 800
860	−0.919±0.09	*39* 850	910	−0.756±0.08	*39* 900
970	−0.637±0.08	*39* 900,1000	1090	−0.507±0.05	*39* 1100
1170	−0.511±0.05	*39* 1100,1200	1210	−0.512±0.05	*39* 1200
1300	−0.527±0.05	*39* 1300	1360	−0.530±0.05	*39* 1300,1400
1410	−0.532±0.05	*39* 1400	1450	−0.531±0.05	*39* 1450
1500	−0.524±0.05	*39* 1500			
		σ_{tot} ($I=0$) (mb)			
600	18.24 ±0.31	*42* 608	650	19.70 ±0.30	*42* 664
700	20.14 ±0.28	*42* 717	800	20.91 ±0.38	*42* 793
860	21.54 ±0.27	*42* 870	910	20.43 ±0.28	*42* 922
970	21.06 ±0.28	*42* 975	1080	24.09 ±0.89	*40* 1091
1210	22.79 ±0.43	*40* 1191,1242	1300	20.74 ±0.39	*40* 1292
1360	20.20 ±0.38	*40* 1342	1410	20.17 ±0.38	*40* 1392
1500	19.98 ±0.34	*40* 1492			
		σ_r ($I=0$) (mb)			
600	0.00 ±0.10		650	0.30 ±0.10	*44* 640
700	0.72 ±0.12	*44* 720	800	0.51 ±0.20	*44* 780
860	1.20 ±0.25	*44* 850	910	2.07 ±0.30	*44* 900
970	3.45 ±0.42	*44* 980	1080	6.83 ±0.70	*44* 1060,1130
1210	9.03 ±0.78	*44* 1210	1300	8.70 ±1.00	*44* 1290
1360	10.02 ±0.88	*44* 1350	1410	10.02 ±0.88	*44* 1420
1500	9.84 ±0.86	*44* 1510			

TABLE I. (*Continued.*)

P_{lab} (MeV/c)	Data	Reference	P_{lab} (MeV/c)	Data	Reference
		Ref(0) (I=0) (fm)[c]			
600	0.279±0.112	*45* 600	650	0.298±0.122	*45* 600,700
700	0.317±0.122	*45* 700	800	0.322±0.124	*45* 800
860	0.309±0.124	*45* 800,900	910	0.301±0.122	*45* 900
970	0.275±0.122	*45* 900,1000	1080	0.227±0.117	*45* 1000,1100
1210	0.040±0.085	*45* 1200	1300	−0.047±0.078	*45* 1300
1360	−0.052±0.078	*45* 1300,1400	1410	−0.055±0.078	*45* 1400
1500	−0.048±0.079	*45* 1500			

[a]Three or four-digit numbers in a reference column are original experimental laboratory momenta in MeV/c. When more than a reference and/or a momentum are shown for a datum, its value is taken by interpolating, averaging, or summing the corresponding original data.
[b]α is the real to imaginary ratio of the forward amplitude. The error is assumed to be 10% for Ref. 39.
[c]Ref(0) denotes the real part of the forward amplitude in the laboratory system, normalized as $\sigma_{tot}=(4\pi/P_{lab})\mathrm{Im}f(0)$.

TABLE II. KN angular data.[a]

P_{lab} (MeV/c)	cosθ	References and comments
	$\sigma(\theta)$ (K^+p)	
600	−0.950—0.925	*30* 603(16); *31* 588(9); *32* 613(20)
650	−0.850—0.780	*22* 642(5); *30* 646(17)
700	−0.973—0.925	*30* 689(17); *32* 726(20)
		34 698(40) cosθ=0.8, 0.18, 0.1, 0.58 deleted
800	−0.850—0.925	*21* 810(7); *24* 780(20); *30* 813(18)
860	−0.9125—0.850	*26* 864(18); *29* 870(16); *30* 857(18)
		33 865(64)
910	−0.973—0.921	*27* 900(19); *29* 910(27); *30* 899(18)
		33 910(66); *34* 909(46) cosθ=−0.58 deleted
970	−0.973—0.926	*23* 970(9); *26* 969(18); *27* 970(19)
		29 970(18); *33* 970(66); *34* 972(47)
1090	−0.972—0.933	*29* 1090(19); *33* 1098(67); *34* 1085(47)
1170	−0.972—0.936	*29* 1170(23); *33* 1170(66); *34* 1169 (47)
1210	−0.972—0.938	*26* 1207(19); *27* 1210(19); *29* 1220(20)
		33 1207(66); *34* 1213(47)
1300	−0.972—0.940	*29* 1320(26); *33* 1310(66); *34* 1301(47)
1360	−0.971—0.963	*27* 1380(19); *29* 1370(19); 33 1370(65)
		34 1373(48)
1410	−0.8875—0.8875	*33* 1400(66)
1450	−0.971—0.965	*29* 1450(15); *33* 1450(66); *34* 1442(48)
1500	−0.971—0.966	*27* 1480(19); *33* 1495(66); *34* 1490(48)
	$P(\theta)$ (K^+p)	
600	−0.80—0.70	*38* 650(16)
650	−0.80—0.70	*38* 650(16)
700	−0.80—0.70	*38* 700(16)
860	−0.81—0.78	*35* 870(17); *38* 845(16)
910	−0.81—0.84	*35* 910(29); *38* 940(16)
970	−0.84—0.80	*35* 970(19)
1090	−0.85—0.85	*35* 1090(22)
1170	−0.84—0.84	*35* 1170(16) seven data cosθ=0.71—0.37 deleted
1210	−0.82—0.83	*35* 1220(21)
1300	−0.91—0.87	*35* 1320(28); *36* 1330(19)
1360	−0.91—0.93	*35* 1370(22); *37* 1370(24)

TABLE II. (*Continued.*)

P_{lab} (MeV/c)	cosθ	References and comments
1410	−0.91—0.93	*35* 1370,1450(43); *36* 1430(19) *37* 1370,1420(45)
1450	−0.91—0.89	*35* 1450(21); *37* 1450(21)
1500	−0.91—0.90	*35* 1450,1540(46); *36* 1540(19) *37* 1450(21)
	$\sigma(\theta)$ ($K^+d\rightarrow K^+np$)	
600	−0.55—0.75	*48* 604(14)
650	−0.95—0.65	*46* 640(17)
700	−0.95—0.75	*46* 720(18); *47* 720(15); *48* 688(15)
800	−0.95—0.75	*46* 780(18)
860	−0.95—0.75	*46* 850(18); *47* 850(15); *48* 853(15)
910	−0.95—0.75	*46* 900(18); *48* 936(15)
970	−0.95—0.75	*46* 980(18)
1080	−0.95—0.75	*46* 1060(18); *47* 1060(15)
1210	−0.95—0.75	*46* 1210(19)
1300	−0.95—0.75	*46* 1290(19)
1360	−0.95—0.85	*46* 1350(19); *47* 1350(15)
1410	−0.95—0.85	*46* 1420(19); *47* 1420(15)
1500	−0.95—0.85	*46* 1510(19)
	$\sigma(\theta)$ ($K^+d\rightarrow K^0pp$)	
600	−0.90—0.90	*50* 600(10); *48* 604(17); *54* 587(10)
650	−0.95—0.95	*49* 641(17); *52* 640(20)
700	−0.95—0.95	*52* 720(20); *53* 720(20); *48* 688(17) *55* 690(20)
800	−0.95—0.95	*49* 811(7); *52* 780(20); *53* 780(9) *55* 790(20)
860	−0.95—0.95	*51* 865(20); *52* 850(20); *53* 850(9) *48* 853(17)
910	−0.95—0.95	*52* 900(20); *53* 900(9); *48* 936(17) *55* 890(20)
970	−0.95—0.95	*51* 970(20); *52* 980(20); *53* 980(10)
1080	−0.95—0.95	*52* 1060(20); *53* 1060(10)
1210	−0.95—0.95	*51* 1210(20); *52* 1210(20); *53* 1210(10)
1300	−0.95—0.95	*52* 1290(20); *53* 1290(10)
1360	−0.95—0.95	*51* 1365(19); *52* 1350(20); *53* 1350(10)
1410	−0.95—0.95	*52* 1420(20); *53* 1420(10)
1500	−0.95—0.95	*52* 1510(20); *53* 1510(10)
	$\sigma(\theta)$ ($K^0_Lp\rightarrow K^+n$)	
600	0.714,0.791	*59* 625(2)
650	−0.450—0.850	*59* 650(15)
800	0.703—0.798	*59* 775(3)
860	−0.550—0.850	*59* 850(14)
910	0.661—0.815	*59* 925(4)
970	−0.550—0.850	*59* 950(14)
1080	−0.550—0.850	*59* 1050(14)
1360	−0.650—0.850	*59* 1350(15)
	$P(\theta)$ (K^+n)	
860	−0.85—0.86	*56* 851(10)
910	−0.85—0.86	*56* 851,965(18)
970	−0.85—0.49	*56* 965(8)
1080	−0.85—0.87	*56* 1064(9); *57* 1060(8)
1210	−0.85—0.88	*56* 1193(9)
1300	−0.70—0.95	*57* 1280(11)

TABLE II. (*Continued.*)

P_{lab} (MeV/c)	cosθ	References and comments
1360	−0.83–0.85	*56* 1351(7); *57* 1390(8)
1410	−0.70–0.80	*57* 1390(8)
1500	−0.30–0.90	*57* 1490(7)
	$P(\theta)$ ($K^+n\to K^0p$)	
600	−0.80–0.55	*50* 600(5)
860	−0.69–0.67	*58* 851(8)
910	−0.70–0.69	*58* 851,965(16)
970	−0.70–0.69	*58* 965(8)
1080	−0.71–0.70	*58* 1064(8); *57* 1060(8)
1210	−0.70–0.69	*58* 1193(7) cos$\theta=-0.49$ deleted
1300	−0.70–0.70	*57* 1280(8)
1360	−0.70–0.70	*58* 1351(7); *57* 1390(8)
1410	−0.70–0.70	*57* 1390(8)
1500	−0.75–0.75	*57* 1490(6)

[a]Three or four-digit numbers in a reference column are original experimental laboratory momenta in MeV/c. Numbers in parentheses denote the number of data points.

Here $\vec{k}$ ($\vec{k}'$) is the incident (scattered) kaon c.m. momentum. The normalization convention is

$$\frac{d\sigma}{d\Omega}=|f|^2+|g|^2, \tag{6}$$

and the optical theorem reads

$$\sigma_{\rm tot}=\frac{4\pi}{k}{\rm Im}f(\theta=0)\ \ [g(\theta=0)=0]\ . \tag{7}$$

The two amplitudes are expanded in partial waves:

$$f^I(\theta)=\frac{1}{k}\sum_{l=0}^{\infty}[(l+1)T^I_{l,l+(1/2)}+lT^I_{l,l-(1/2)}]P_l(\cos\theta) \tag{8}$$

and

$$g^I(\theta)=\frac{1}{k}\sum_{l=0}^{\infty}(T^I_{l,l+(1/2)}-T^I_{l,l-(1/2)})\times\sin\theta\frac{dP_l(\cos\theta)}{d\cos\theta}\ . \tag{9}$$

Each partial wave $T^I_{l,j=l\pm(1/2)}$ is parametrized by the real phase shift δ^I_{lj} and the absorption parameter η^I_{lj} ($0\le\eta\le1$) as follows:

$$T^I_{lj}=\frac{1}{2i}[\eta^I_{lj}\exp(2i\delta^I_{lj})-1]\ . \tag{10}$$

Possible spin observables in the spin-0 spin-$\frac{1}{2}$ system are schematically shown in Fig. 1. The expression of the polarization parameter P is

$$\frac{d\sigma}{d\Omega}P=2\,{\rm Im}(fg^*)\ . \tag{11}$$

The other spin observables have not been available since they require the measurement of the recoiled nucleon polarization. Expressions of them are combined in a matrix notation:

$$\frac{d\sigma}{d\Omega}\begin{bmatrix}R\\A\end{bmatrix}=\begin{bmatrix}\cos\alpha & -\sin\alpha\\ \sin\alpha & \cos\alpha\end{bmatrix}\begin{bmatrix}|f|^2-|g|^2\\ -2\,{\rm Re}(fg^*)\end{bmatrix}, \tag{12}$$

where

$$\alpha=\theta_r^*-\theta_r\ . \tag{13}$$

θ_r^* and θ_r are the nucleon recoil angles in the c.m. and laboratory system, respectively. Note that $P^2+R^2+A^2=1$.

The amplitudes f and g in Eqs. (8) and (9) have to be modified for K^+p scattering if we take the Coulomb interaction into account. In the present work we employ the following expression for the Coulomb correction:

$$f(K^+p)=\frac{1}{k}\sum_{l=0}^{\infty}[(l+1)T^1_{l,l+(1/2)}+lT^1_{l,l-(1/2)}]\times e^{2i\Phi_l}P_l(\cos\theta)+f_C \tag{8'}$$

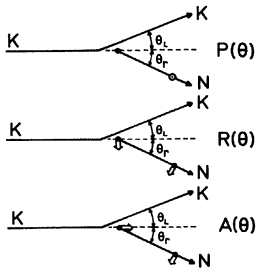

FIG. 1. Polarization and spin rotation parameters. Arrows represent the spin orientation of nucleons. ⊙ is an arrow out of the page.

and

$$g(\mathrm{K}^+\mathrm{p})=\frac{1}{k}\sum_{l=0}^{\infty}(T^1_{l,l+(1/2)}-T^1_{l,l-(1/2)} \times e^{2i\Phi_l}\sin\theta\frac{dP_l(\cos\theta)}{d\cos\theta}\ , \tag{9'}$$

where f_C is the Coulomb amplitude and Φ_l are the Coulomb phase shifts, which are, respectively, defined as

$$f_C=\frac{\alpha}{2kv\sin^2(\theta/2)}\exp\left[-i\frac{\alpha}{v}\ln\left[\sin^2\frac{\theta}{2}\right]\right] \tag{14}$$

and

$$\Phi_l=\sum_{n=1}^{l}\tan^{-1}\frac{\alpha}{nv}\ . \tag{15}$$

Here v is the relative velocity between the kaon and nucleon, and $\alpha\simeq 1/137$.

B. Kd breakup reaction formulas

Since the available K$^+$n scattering data are inferred from deuteron experiments, the neutron binding in the deuteron has to be isolated to deduce the KN scattering parameters. In the present analysis we essentially follow the formulas developed by Stenger *et al.*[62] and Alberi *et al.*[63] Formulas are simplified from those of Alberi but use fully relativistic kinematics, unlike the calculation by Stenger *et al.*

In the impulse approximation, applied to the present K$^+$d system, we assume that the incident kaon interacts with one of the nucleons in the deuterium nucleus while the other nucleon is a spectator to the interaction. The spectator can contribute to the entire process only kinematically through the deuteron structure in the initial state and the final three-body phase space configuration. Possible distortions owing to the interaction between the final nucleons and double scattering of the kaon from the nucleons are neglected. The applicability of the above assumption to the K$^+$d system can be justified for two reasons:

(1) The deuteron can be considered as a loosely bound system of the proton and neutron (B=2.2 MeV).

(2) The nuclear mean free path of K$^+$ is about 5–7 fm,[5] which is sufficiently long to neglect double scattering and absorption of K$^+$ in the deuteron interior.

The kinematics of the reaction is shown in Fig. 2. The amplitude T corresponding to Fig. 2 can be written as follows:[63]

$$T=\sqrt{16\pi^3 M}\,[T_{\mathrm{N}}(q)u(p)+T_{\mathrm{N}}(p)u(q)]\ , \tag{16}$$

where u is the deuteron wave function in momentum space, T_{N} is the KN amplitude, and M is the deuteron mass. The overall normalization factor can be obtained by considering the low energy scattering theory with bound states.[63,64]

We notice that the KN amplitude in Eq. (16), T_{N}, is in general unphysical since the interacting nucleon is off the mass shell. However, we can substitute T_{N} with a physical amplitude as a fair approximation. This can be justified as follows: The deuteron wave function in Eq. (16) decreases very rapidly when its argument becomes large. Therefore, in an integration over the final three-body phase space, the main contribution to the cross section comes from configurations near zero spectator momentum, at which T_{N} is the physical laboratory amplitude if we neglect the deuteron binding energy and the mass difference of the neutron and the proton.

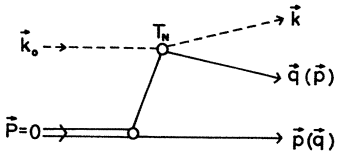

FIG. 2. Kinematics for deuteron breakup reactions. The kaon and nucleon are denoted by dashed and solid lines, respectively.

To deduce the KN c.m. scattering cross section from the breakup events, we have to define the KN two-body c.m. system in the breakup kinematics. There is, however, no standard way to do this. A reasonable definition would be to refer to the final KN system after identifying the spectator nucleon. However, as has been assumed so far, it is sufficient to develop a formalism for negligible spectator momenta. So, we simply evaluate T_{N} at the stationary spectator configuration.[65]

By the approximation described above, the differential cross sections for the breakup reactions, with and without charge exchange, can be expressed in terms of the KN amplitudes and the form factors (we neglect the D-wave component of the deuteron wave function):

$$\frac{d\sigma}{d\Omega}(\mathrm{K}^+\mathrm{d}\to\mathrm{K}^0\mathrm{pp})=(|f_x|^2+|g_x|^2)[I(\theta)-J(\theta)] +\tfrac{2}{3}|g_x|^2J(\theta) \tag{17}$$

and

$$\frac{d\sigma}{d\Omega}(\mathrm{K}^+\mathrm{d}\to\mathrm{K}^+\mathrm{np})=(|f_{\mathrm{p}}|^2+|g_{\mathrm{p}}|^2)I_{\mathrm{n}}(\theta) +(|f_{\mathrm{n}}|^2+|g_{\mathrm{n}}|^2)I_{\mathrm{p}}(\theta) +2\,\mathrm{Re}(f^*_{\mathrm{p}}f_{\mathrm{n}}+\tfrac{1}{3}g^*_{\mathrm{p}}g_{\mathrm{n}})J(\theta)\ , \tag{18}$$

where f_{p}, f_{n}, and f_x are the spin non-flip amplitudes for K$^+$p elastic, K$^+$n elastic, and K$^+$n charge exchange scattering, respectively. The g's are the corresponding spin-flip amplitudes. The deuteron inelastic form factors are expressed by I and J. The subscript I in Eq. (18) specifies the spectator nucleon. If one does not distinguish a spectator nucleon from the other, the I-type form factors are identical, i.e., $I_{\mathrm{p}}=I_{\mathrm{n}}=I$. However, in experiments we do distinguish it. In this case we have to calculate the form factors I_{p} and I_{n} separately. Here we show general expressions for I and J without the spectator specification:

$$I(\theta)=K\int\frac{k^2dk}{\omega}\frac{d^3p}{E_p}\frac{d^3q}{E_q}\delta^4(k_0+P-k-p-q)\times\frac{u^2(p)+u^2(q)}{2} \quad (19)$$

and

$$J(\theta)=K\int\frac{k^2dk}{\omega}\frac{d^3p}{E_p}\frac{d^3q}{E_q}\delta^4(k_0+P-k-p-q)\times u(p)u(q)\ , \quad (20)$$

where

$$K=\frac{\omega}{k^2}\frac{d(\omega+E_q)}{dk}mE_q\bigg|_{p=0} \quad (21)$$

and

$$\omega=\sqrt{k^2+\mu^2},\quad E_p=\sqrt{p^2+m^2},\quad E_q=\sqrt{q^2+m^2}\ . \quad (22)$$

Here μ and m are, respectively, the kaon and nucleon masses. The factor K comes from the transformation of the kaon scattering angle from the laboratory to the c.m. frame of the KN two-body system. As assumed above, K is evaluated at the stationary spectator configuration.[65]

The form factors I and J contain information on the deuteron internal structure, the final three-body phase space, and the Pauli exclusion principle for Eq. (17), as the general requirements of the assumed framework. In addition, these form factors can reflect specific information on the individual experiments. This point has to be discussed more by referring to actual experimental data-taking procedures.

To obtain KN two-body scattering cross sections from observed breakup events, most experiments define the spectator nucleon in the final state. Certain criteria are employed for the definition, and event selections are made according to them. The most common way of doing this is to impose a momentum cutoff of one nucleon in the final state. In the spirit of the impulse approximation, the spectator nucleon emerges in the final state with the momentum expected from the Fermi motion. The Fermi momentum of the nucleon should not be larger than about 200 or 300 MeV/c for the deuteron. If it were larger, the final state interaction and/or the double scattering effect would be a major distortion. Since each experiment adopts different criteria for the event selection and this may affect the form factors through the phase space factor, we cannot apply a common formula, but a consideration is needed for the individual experiments.

As shown in Eq. (17), the reaction $K^+d\to K^0pp$ consists of only one KN process, namely, $K^+n\to K^0p$. Therefore, the correction is merely kinematical provided the impulse approximation is correct. In bubble chamber experiments an outgoing K^0 is identified by the $\pi^+\pi^-$ decay vertex (often referred to as a "vee"). The rest of the system, which contains two protons, may create two traces (a two-pronged event) or only one (a one-pronged event). If one of the protons has sufficiently small momentum, it may not leave a trace in the chamber. The limit of the visibility is reported as 100 MeV/c.[46] Therefore, the measurements for the one-pronged events are considered to impose the upper cutoff of 100 MeV/c automatically. For two-pronged measurements,[52] on the contrary, the limit imposes a lower cutoff. An additional momentum cutoff is also imposed on the slower proton.[50,52–55]

Equation (18) is composed of the three terms corresponding to K^+p, K^+n scattering, and their interference. Therefore, the K^+n scattering cross sections cannot be extracted kinematically from the breakup events. In general we have to consider all three terms in Eq. (18).

In experiments the outgoing K^+ is identified by the three charged pion decay, which is very characteristic for K^+ (the τ decay). The remaining two-nucleon system can contain p and n or d. Since n cannot be measured directly, the outgoing proton or deuteron may be seen (a two-pronged vertex) or may not (a one-pronged vertex). The contamination of K^+d elastic scattering would be large in a very forward region[66] (largely diffractive scattering), so there are few forward data and, if any, they are very erroneous.

The experiment in Ref. 48 makes no momentum check for the final n-p system. (We use the data in Ref. 48 for $K^+d\to K^+np$ or d as discussed in the preceding section.) In this case the form factors I_n and I_p are identical since the present formula must be the same for the proton and neutron.[67] The experiments by the BGRT collaboration impose the condition on the proton momentum by selecting one-pronged events[47] and two-pronged events.[46] In these cases, the form factors I_n and I_p are not the same, but $I_n<I_p$. In addition to the above constraint on the proton momentum, it is also important that the BGRT experiments[46,47] fit the neutron momentum and impose the condition $P_p<P_n$ when selecting events.

The above constraints on the spectator momentum affect the form factors through the final three-body phase space integration. We can take these constraints in Eqs. (19) and (20) by changing the integration range. In Fig. 3 we plot $I(\theta)$ and $J(\theta)$ for various conditions of the spectator momentum calculated with the use of the S-wave part of the Hamada-Johnston deuteron wave function.[68]

The form factor J, which represents the interference between the interactions of the kaon with the two nucleons, is appreciable only at very forward angles. The momentum cutoff effectively suppresses J. Especially J is essentially zero in the entire angle range for the reaction $K^+d\to K^+np$, in which the condition $P_p<P_n$ turns out to be effective in this suppression.

The form factor I is almost constant. For one-pronged measurements ($0<P_{spec}<100$ MeV/c), the momentum cutoff suppresses the form factor I (and hence the cross sections) by 25%. The suppression exceeds even 75% for the momentum cutoff of $100<P_{spec}<250$ MeV/c. Therefore, when an experiment adopts the momentum cutoff, it always suffers from a normalization problem. Such experiments renormalize the obtained angular distribution so that it gives the integrated cross section the same value as that obtained from the unconstrained events,[46,47,52,53,55] or a value taken from other experiments.[50] Therefore, the calculated form factors have to be also renormalized. The factor to normalize the constrained cross section to unconstrained events is more than 4 for the two-pronged mea-

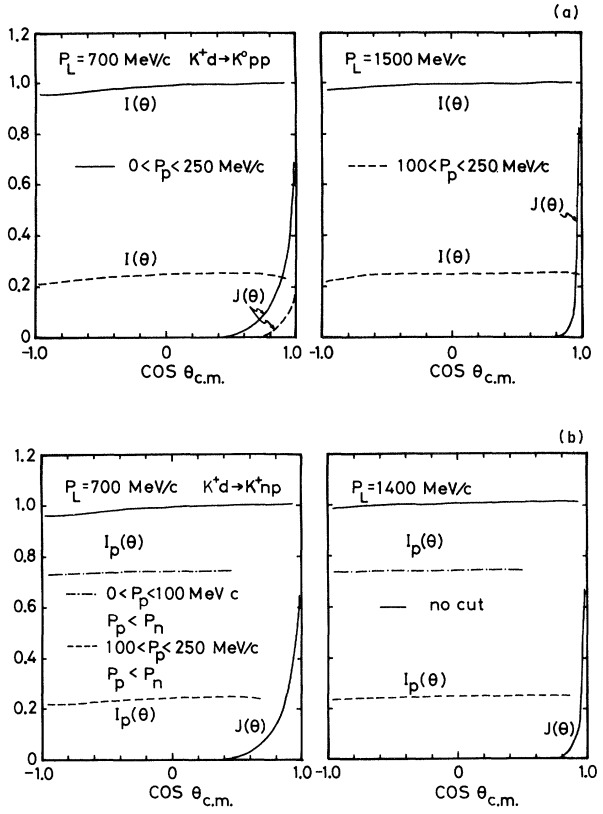

FIG. 3. (a) Deuteron inelastic form factors for $K^+d \to K^0pp$. $I(\theta)$ and $J(\theta)$ in Eq. (17) are plotted at 700 and 1500 MeV/c vs $\cos\theta_{c.m.}$, which is determined for the stationary spectator configuration. The momentum cutoff is $0 < P_p < 250$ MeV/c (solid curves) and $100 < P_p < 250$ MeV/c (dashed curves), where P_p is the momentum of the slower proton. (b) Deuteron inelastic form factors for $K^+d \to K^+np$. $I_p(\theta)$ and $J(\theta)$ in Eq. (18) are plotted at 700 and 1500 MeV/c. Solid curves are calculated without introducing the momentum cutoff, in which case $I_p = I_n$. Dashed curves are calculated under the condition $100 < P_p < 250$ MeV/c, and dash-dotted curves are for $0 < P_p < 100$ MeV/c. In both cases the additional condition $P_p < P_n$ is imposed. The form factors J and I_n which are not plotted are negligible on this scale.

surements. Thus the breakup data are subject to a large normalization uncertainty in addition to that of the flux normalization. This uncertainty has to be properly dealt with in the analysis.

IV. METHOD

The analysis employs an orthodox single energy method in which solutions are searched separately at discrete energy points. Some of the recent KN analyses[45,61,69–71] are energy dependent using a flexible model function for the energy dependence of the amplitude or impose constraints to obtain a smooth solution. In the single energy analysis, we assume no additional parametrization. Therefore, the result could be free from possible biases owing to a particular functional form or a model.

The analysis points are taken at 600, 650, 700, 800, 860, 910, 970, 1080, 1170, 1210, 1300, 1360, 1410, 1450, and 1500 MeV/c. These are chosen empirically concerning that there are sufficient data around a momentum point within the momentum bin of 20 MeV/c. The simultaneous analysis for the $I=1$ and $I=0$ states is possible at most of the above momenta.[72]

At each momentum point of the analysis, there may be several solutions corresponding to possible minima of χ^2 in parameter space. This is the rather general case in amplitude analyses if the experimental information is poor qualitatively and/or quantitatively. A "true" solution, therefore, has to be selected among the possibilities by a certain criterion. In the single energy method a solution is selected which provides smooth energy dependence relative to other solutions at different energies. Since we refer to the energy dependence of all the free parameters, this selection could exclude many "wrong" possibilities.

The search was started from the amplitude obtained by Martin and Oades (MO).[70] Their work is one of the most recent analyses performed in the KN $I=1$ and $I=0$ states simultaneously. Obtained solutions sometimes differ from the initial values significantly because the MO analysis employs the fixed-t dispersion relation as a constraint.[70] These primitive solutions have been refined through the following procedures: The amplitude is determined at the lowest momentum, 600 MeV/c. At this momentum the amplitude is consistent among recent analyses, and with the present result. Solutions at the next higher momentum, 650 MeV/c, are searched for by starting from the previous solution and by finding possible nearby minima of χ^2. Acceptable solutions can be selected among them requiring smooth energy dependence of partial waves. Similarly the search is continued up to the highest momentum.

After the above cycle, problems with fitting certain experimental data were checked, which are most likely incorrect normalization, underestimation of the statistical errors, etc. Also, by the very nature of the single energy analysis, an accidental structure of the data base would probably be reflected in the behavior of the amplitudes, especially of higher partial waves. Such an undesirable structure is often created by using an experiment which is inconsistent with others. The inconsistency can be checked according to the quality of the fit and to the amplitude currently obtained. Then the previous cycle is repeated until no more improvement seems to be necessary or possible.

Differential cross section data are renormalized in the course of the analysis. The renormalization is done at least once for one solution at a given momentum. The normalization error is assumed to be 5% for the K^+p and 10% for the K^+d breakup reaction cross sections. For the cross sections of $K_L^0 p \to K^+n$, the error of 25% is assumed. The final employed normalization factors are listed in Table III.

As discussed in Sec. III, renormalization for the deuteron inelastic form factors is also necessary for some breakup reaction experiments. The normalization factors are calculated as the reciprocal of the data normalization factors for the corresponding experiments. These factors are also listed in Table III.

TABLE III. Normalization for differential cross sections.[a]

P_{lab} (MeV/c)	Reference	N_d	N_f	P_{lab} (MeV/c)	Reference	N_d	N_f
			$\sigma(\theta)$ (K^+p)				
600	*30* 603	1.0062		650	*22* 642	1.0054	
	31 588	0.9682			*30* 646	1.0189	
	32 613	1.0310					
700	*30* 689	0.9922		800	*21* 810	0.9697	
	32 726	0.9824			*24* 780	0.9697	
	34 698	0.9660			*30* 813	0.9799	
860	*26* 864	0.9625		910	*27* 900	0.9838	
	29 870	0.9890			*29* 910	1.0090	
	30 857	0.9712			*30* 899	0.9621	
	33 865	0.9933			*33* 910	1.0267	
970	*23* 970	1.0433			*34* 909	0.9453	
	26 969	0.9307		1090	*29* 1090	0.9658	
	27 970	0.9439			*33* 1098	0.9810	
	29 970	0.9825			*34* 1085	0.9540	
	33 970	0.9626		1210	*26* 1207	0.9782	
	34 972	0.9276			*27* 1210	0.9693	
1170	*29* 1170	1.0190			*29* 1220	1.0093	
	33 1170	0.9651			*33* 1207	0.9988	
	34 1169	0.9142			*34* 1213	0.9539	
1300	*29* 1320	0.9652		1360	*27* 1380	0.9603	
	33 1310	0.9968			*29* 1370	1.0299	
	34 1301	0.9124			*33* 1370	1.0094	
1410	*33* 1400	1.0035			*34* 1373	0.9479	
1450	*29* 1450	1.0183		1500	*27* 1480	0.9494	
	33 1450	1.0288			*33* 1495	0.9920	
	34 1442	0.9113			*34* 1490	0.9230	
			$\sigma(\theta)$ ($K^+d \rightarrow K^+np$)				
600	*48* 604	0.9889	1.0	650	*46* 640	1.0	3.4720
700	*46* 720	1.0	3.7832	800	*46* 780	1.0	3.9702
	47 720	1.0	1.1399	860	*46* 850	1.0	4.0427
	48 688	1.0039	1.0		*47* 850	1.0	1.2362
910	*46* 900	1.0	4.1862		*48* 853	1.0980	1.0
	48 936	0.9615	1.0	970	*46* 980	1.0	4.0851
1080	*46* 1060	1.0	4.7536	1210	*46* 1200	1.0	4.1032
	47 1060	1.0	1.5522	1300	*46* 1290	1.0	3.8832
1360	*46* 1350	1.0	4.3317	1410	*46* 1420	1.0	4.1636
	47 1350	1.0	1.4792		*47* 1420	1.0	1.4552
1500	*46* 1510	1.0	4.0102				
			$\sigma(\theta)$ ($K^+d \rightarrow K^0pp$)				
600	*50* 600	0.9955	1.0	650	*49* 641	1.0180	1.0
	48 604	1.0044	1.0		*52* 640	1.0198	1.0
	54 587	1.0002	1.0				
700	*52* 720	1.0103	1.0	800	*49* 811	1.0263	1.0
	53 720	1.0	3.9482		*52* 780	0.9656	1.0
	48 688	1.0186	1.0		*53* 780	1.0	4.2209
	55 690	0.9813	1.0		*55* 790	0.9907	1.0
860	*51* 865	0.9472	1.0	910	*52* 900	0.9431	1.0
	52 850	0.9794	1.0		*53* 900	1.0	4.3318
	53 850	1.0	4.1837		*48* 936	0.9632	1.0
	48 853	0.9933	1.0		*55* 890	0.9339	1.0
970	*51* 970	0.9655	1.0	1080	*52* 1060	1.0	1.1765
	52 980	0.9464	1.0		*53* 1060	1.0	4.6357
	53 980	1.0	4.3119				
1210	*51* 1210	0.9617	1.0	1300	*52* 1290	1.0	1.1121
	52 1210	1.0	1.0875		*53* 1290	1.0	4.3831

TABLE III. (*Continued.*)

P_{lab} (MeV/c)	Reference	N_d	N_f	P_{lab} (MeV/c)	Reference	N_d	N_f
	53 1210	1.0	4.3897				
1360	*51* 1365	0.8942	1.0	1410	*52* 1420	0.9465	1.0
	52 1350	1.0	1.1274		*53* 1420	1.0	4.1963
	53 1350	1.0	4.4736				
1500	*52* 1510	1.0	1.1606				
	53 1510	1.0	4.4286				
			$\sigma(\theta)$ ($K_L^0 p \to K^+ n$)				
600	*59* 625	0.7998		650	*59* 650	0.8420	
800	*59* 775	0.8062		860	*59* 850	0.6251	
910	*59* 925	0.8005		970	*59* 950	0.6212	
1080	*59* 1050	0.6749		1360	*59* 1350	1.0647	

[a]Normalization factors are denoted by N_d and N_f, which are for experimental data and the deuteron form factors, respectively. Four- and three-digit numbers in a reference column are original experimental laboratory momenta in MeV/c.

TABLE IV. KN phase shifts.[a]

	$I=1$		$I=0$	
L_{2j}	δ	η	δ	η
		600 MeV/c $\chi^2=101.17$ 125 data		
S_1	−28.1526±0.7017	1.0000±0.0	−18.2288±0.8868	1.0000±0.0
P_1	−13.6416±0.8880	1.0000±0.0	36.0717±0.6200	1.0000±0.0
P_3	6.8424±0.3680	1.0000±0.0	−1.7686±0.8307	1.0000±0.0
D_3	−0.2622±0.3343	1.0000±0.0	3.9428±0.4675	1.0000±0.0
D_5	−1.9069±0.3077	1.0000±0.0	−0.9465±0.5292	1.0000±0.0
F_5	−0.1684±0.2111	1.0000±0.0	0.3965±0.5673	1.0000±0.0
F_7	0.4865±0.1538	1.0000±0.0	−0.1298±0.3847	1.0000±0.0
		650 MeV/c $\chi^2=97.90$ 103 data		
S_1	−29.0513±0.4112	1.0000±0.0	−19.3140±0.8118	1.0000±0.0
P_1	−15.7442±0.5245	1.0000±0.0	40.2641±0.6306	1.0000±0.0
P_3	7.5035±0.2687	1.0000±0.0	−4.6549±0.5058	1.0000±0.0
D_3	0.0480±0.2733	1.0000±0.0	5.8511±0.3787	1.0000±0.0
D_5	−3.0780±0.2033	1.0000±0.0	−0.8962±0.4305	1.0000±0.0
		700 MeV/c $\chi^2=181.78$ 213 data		
S_1	−29.7733±0.3934	1.0000±0.0	−20.3180±0.8772	1.0000±0.0
P_1	−17.8140±0.4161	0.9930±0.0014	42.4710±0.7495	1.0000±0.0
P_3	8.5847±0.2395	1.0000±0.0	−4.0031±0.5760	1.0000±0.0
D_3	0.5050±0.2587	1.0000±0.0	6.7712±0.3540	1.0000±0.0
D_5	−2.6729±0.2073	1.0000±0.0	−1.1099±0.3465	0.9834±0.018
F_5	−0.5887±0.2165	1.0000±0.0	0.4471±0.3413	1.0000±0.0
F_7	0.9531±0.1417	1.0000±0.0	−1.0613±0.3109	1.0000±0.0
		800 MeV/c $\chi^2=85.87$ 128 data		
S_1	−32.6138±1.4752	1.0000±0.0	−19.2119±2.3989	1.0000±0.0
P_1	−19.6043±1.9750	0.9213±0.0067	51.9807±1.8557	1.0000±0.0
P_3	10.3946±0.7684	1.0000±0.0	−6.6729±1.1967	1.0000±0.0
D_3	−0.1318±0.9935	1.0000±0.0	8.8709±0.8735	1.0000±0.0
D_5	−3.3642±0.8076	1.0000±0.0	−0.7264±0.9747	0.9855±0.0037
F_5	−0.4142±0.4903	1.0000±0.0	1.5900±0.6627	1.0000±0.0
F_7	1.0064±0.3671	1.0000±0.0	0.0815±0.5925	1.0000±0.0

TABLE IV. (*Continued.*)

	$I=1$		$I=0$	
L_{2j}	δ	η	δ	η
	860 MeV/c $\chi^2=340.78$ 301 data			
S_1	−38.5034±0.8487	1.0000±0.0	−20.3008±1.0002	1.0000±0.0
P_1	−13.9702±1.2339	0.8773±0.0070	52.3307±1.0667	1.0000±0.0
P_3	11.0591±0.3938	0.9818±0.0036	−8.5239±0.7444	1.0000±0.0
D_3	−1.0663±0.3746	1.0000±0.0	9.9622±0.4073	1.0000±0.0
D_5	−1.8276±0.2899	1.0000±0.0	−1.3960±0.5784	0.9453±0.0048
F_5	−0.7640±0.1537	1.0000±0.0	2.0523±0.3529	1.0000±0.0
F_7	1.2467±0.2431	1.0000±0.0	−0.4048±0.3790	1.0000±0.0
G_7	−0.4592±0.1161	1.0000±0.0	−0.6301±0.2714	1.0000±0.0
	910 MeV/c $\chi^2=371.96$ 364 data			
S_1	−39.5698±0.7020	1.0000±0.0	−20.3307±1.0559	1.0000±0.0
P_1	−14.7304±1.0185	0.8648±0.0079	49.6957±1.5859	1.0000±0.0
P_3	12.9585±0.3125	0.9425±0.0043	−11.0988±0.9852	1.0000±0.0
D_3	−1.4409±0.3833	1.0000±0.0	10.7080±0.3993	0.9438±0.0306
D_5	−1.7975±0.2533	1.0000±0.0	−1.0000±0.0	0.9521±0.0218
F_5	−0.9109±0.1171	1.0000±0.0	2.9174±0.3450	1.0000±0.0
F_7	0.7338±0.1980	1.0000±0.0	−1.8800±0.3594	1.0000±0.0
	970 MeV/c $\chi^2=321.46$ 300 data			
S_1	−39.2213±1.4039	0.9000±0.0	−21.9615±4.4781	1.0000±0.0
P_1	−18.6516±1.5161	0.8232±0.0263	48.7363±7.8320	0.9587±0.0677
P_3	14.6946±0.5915	0.8788±0.0126	−10.1126±3.1868	1.0000±0.0
D_3	−2.0973±0.5053	1.0000±0.0	15.1055±0.7502	0.8472±0.0916
D_5	−3.2284±0.3822	1.0000±0.0	1.1415±0.6531	0.9659±0.0738
F_5	−0.3132±0.1729	1.0000±0.0	5.7556±0.8613	1.0000±0.0
F_7	0.1435±0.2950	1.0000±0.0	−2.0041±0.4676	1.0000±0.0
	1090 MeV/c $\chi^2=169.82$ 158 data		1080 MeV/c $\chi^2=115.55$ 113 data[b]	
S_1	−45.9048±5.1697	0.6241±0.1777	−24.6430±2.4297	1.0000±0.0
P_1	−26.3255±3.7525	0.7291±0.1245	47.3270±2.9641	0.9510±0.0270
P_3	14.1740±1.5412	0.8781±0.0894	−10.3602±1.7206	1.0000±0.0
D_3	−3.9064±0.9802	1.0000±0.0	15.9553±1.2550	0.7654±0.0548
D_5	−4.1205±0.9803	1.0000±0.0	−2.4220±0.5865	0.9088±0.0232
F_5	−1.8177±0.8609	1.0000±0.0	5.6088±0.4878	1.0000±0.0
F_7	1.4954±0.5797	0.9794±0.0150	−2.1962±0.5572	0.9428±0.0199
G_7	−0.0204±0.3505	1.0000±0.0	1.4226±0.5244	1.0000±0.0
	1170 MeV/c $\chi^2=188.08$ 155 data			
S_1	−51.5724±13.977	0.7120±0.2312		
P_1	−22.4771± 6.8108	0.6307±0.1081		
P_3	11.7034± 3.6594	0.8230±0.1190		
D_3	−7.6412± 3.1816	1.0000±0.0		
D_5	−2.5635± 1.1368	1.0000±0.0		
F_5	−2.2858± 1.2048	1.0000±0.0		
F_7	0.9395± 0.5607	0.9481±0.0370		
G_7	0.2760± 0.4788	1.0000±0.0		
	1210 MeV/c $\chi^2=234.78$ 283 data			
S_1	−45.3483±1.7164	0.7697±0.0638	−25.3726±2.3083	1.0000±0.0
P_1	−31.5631±1.5115	0.7781±0.0372	48.7148±3.3150	0.8760±0.0346
P_3	11.3531±0.7344	0.8476±0.0496	−14.9719±1.8105	1.0000±0.0
D_3	−8.9083±1.1149	1.0000±0.0	10.2863±1.3863	0.6329±0.0637
D_5	−1.6658±0.3104	1.0000±0.0	−2.8329±0.8002	0.9519±0.0296
F_5	−2.9122±0.2981	0.9518±0.0088	5.3900±0.6314	1.0000±0.0
F_7	2.0014±0.2672	0.9138±0.0105	−1.3702±0.7809	0.8625±0.0299
G_7	1.1659±0.1970	1.0000±0.0	3.3047±0.7521	1.0000±0.0

TABLE IV. (*Continued.*)

	$I=1$		$I=0$	
L_{2j}	δ	η	δ	η
		1300 MeV/c $\chi^2=231.62$ 260 data		
S_1	−49.0149±2.2212	0.5445±0.0986	−36.3807±1.6112	1.0000±0.0
P_1	−37.9008±2.5295	0.7967±0.0584	33.7186±4.4675	0.5086±0.0605
P_3	10.7895±1.0713	0.8770±0.0659	−17.4262±1.2294	1.0000±0.0
D_3	−10.4753±1.2336	0.9350±0.0375	7.2264±1.4216	0.7901±0.0483
D_5	−2.4806±0.4943	0.9566±0.0385	−4.9951±0.8064	0.8686±0.0352
F_5	−2.5162±0.7055	0.9631±0.0178	6.3264±0.6606	1.0000±0.0
F_7	2.3321±0.3124	0.9360±0.0190	0.6635±0.7519	0.8879±0.0228
G_7	0.5220±0.4330	1.0000±0.0	5.0236±0.5645	1.0000±0.0
		1360 MeV/c $\chi^2=364.23$ 331 data		
S_1	−47.3673±2.5741	0.4845±0.2710	−31.3035±4.6386	1.0000±0.0
P_1	−42.1863±7.3512	0.7655±0.1201	32.4262±6.0545	0.5677±0.0747
P_3	9.6627±1.6984	0.8739±0.1505	−16.7838±1.5859	0.9216±0.0916
D_3	−11.1751±2.0488	0.9010±0.0691	8.6151±1.8977	0.7215±0.0637
D_5	−2.5106±0.9757	0.9666±0.0432	−2.0444±0.7889	0.9279±0.0430
F_5	−3.2076±1.4802	0.9584±0.0183	7.2973±1.3623	0.9866±0.0374
F_7	2.4546±0.4881	0.9345±0.0423	−0.9858±0.9849	0.8347±0.0299
G_7	0.7165±0.7027	1.0000±0.0	4.5183±0.7223	1.0000±0.0
G_9	−0.0170±0.5109	1.0000±0.0	1.0098±0.5367	1.0000±0.0
		1410 MeV/c $\chi^2=231.22$ 259 data		
S_1	−40.3287±3.1144	0.4655±0.1293	−32.4063±2.5399	1.0000±0.0
P_1	−39.2491±3.0246	0.7216±0.0701	31.0538±3.7266	0.5411±0.0478
P_3	12.4633±0.9381	0.9446±0.0937	−20.0340±1.8788	0.7915±0.0574
D_3	−17.4766±1.2151	0.8072±0.0446	5.7798±1.2255	0.7955±0.0616
D_5	−0.6122±0.9535	1.0000±0.0	1.0105±0.7319	0.9329±0.0462
F_5	−3.1779±1.0294	0.9258±0.0099	10.7139±0.8655	1.0000±0.0
F_7	−0.1787±0.5310	0.9272±0.0079	−1.4584±0.7690	0.8389±0.0268
G_7	−1.2311±0.4550	1.0000±0.0	3.4729±0.5855	1.0000±0.0
G_9	1.4963±0.2008	1.0000±0.0	−2.3847±0.5067	1.0000±0.0
		1450 MeV/c $\chi^2=138.87$ 174 data		
S_1	−42.2579±1.8633	0.5714±0.0285		
P_1	−38.5603±0.5486	0.9383±0.0347		
P_3	14.1638±0.6129	0.6431±0.0150		
D_3	−9.1425±0.7710	0.7897±0.0207		
D_5	−1.7002±0.2811	0.9981±0.0031		
F_5	−1.4420±0.3253	0.9996±0.0024		
F_7	1.5516±0.2735	0.9258±0.0081		
G_7	−0.5770±0.2060	1.0000±0.0		
G_9	−0.1278±0.2371	1.0000±0.0		
		1500 MeV/c $\chi^2=270.63$ 287 data		
S_1	−36.1378±1.9389	0.6168±0.1166	−26.0642±2.9600	1.0000±0.0
P_1	−37.9434±2.4475	0.9997±0.0645	42.3513±7.9844	0.3110±0.1000
P_3	15.5930±0.9954	0.6728±0.0959	−14.7752±2.1861	0.7483±0.0842
D_3	−13.6280±1.4316	0.8224±0.0436	8.9506±1.9369	0.7579±0.0739
D_5	−0.5918±1.2141	1.0000±0.0	−2.6451±1.5309	0.7902±0.0561
F_5	−2.3684±0.6004	0.9280±0.0290	9.5460±1.2279	1.0000±0.0
F_7	0.1659±0.8584	0.9054±0.0138	−5.3994±0.8215	0.8984±0.0356
G_7	0.4993±0.4923	1.0000±0.0	3.2893±0.8388	1.0000±0.0
G_9	0.9634±0.4674	1.0000±0.0	0.6702±0.6324	1.0000±0.0

[a]The real phase shift δ is given in degrees. Parameters with zero errors are fixed to indicate values.
[b]The analysis at 1080 MeV/c is made at 1090 MeV/c for the $I=1$ state, while the $I=0$ state is analyzed at 1080 MeV/c with the $I=1$ amplitude fixed to the values at 1090 MeV/c.

V. RESULTS

The final obtained phase parameters are listed in Table IV. The error values are estimated from the error matrix, which can be calculated in the course of the minimization. The higher partial wave amplitudes with $l \geq 5$ and inelasticity for $l \geq 4$ are assumed to be zero. Argand diagrams for some partial waves are plotted in Fig. 4, where the results of the present analysis are shown both in a discrete and a continuous manner. The continuous lines are drawn by sight assuming smooth energy dependence of the real and imaginary parts of the partial waves. Although the lines are ambiguous at the highest few momenta, they could represent typical behavior of the partial wave amplitudes. The results of other recent KN analyses[70,71] are also plotted in Fig. 4 for comparison.

Figure 5 collects the fit to some data by the present solution. In Fig. 5(a) the new polarization data are plotted.[56–58] The fits to the breakup reaction cross sections are shown in Figs. 5(b) and (c).

As discussed in the preceding section, the Rutherford data[48] are for unconstrained events ($K^+d \rightarrow K^+np$ or K^+d). They are well fitted consistently with the other bubble chamber data.[46,47]

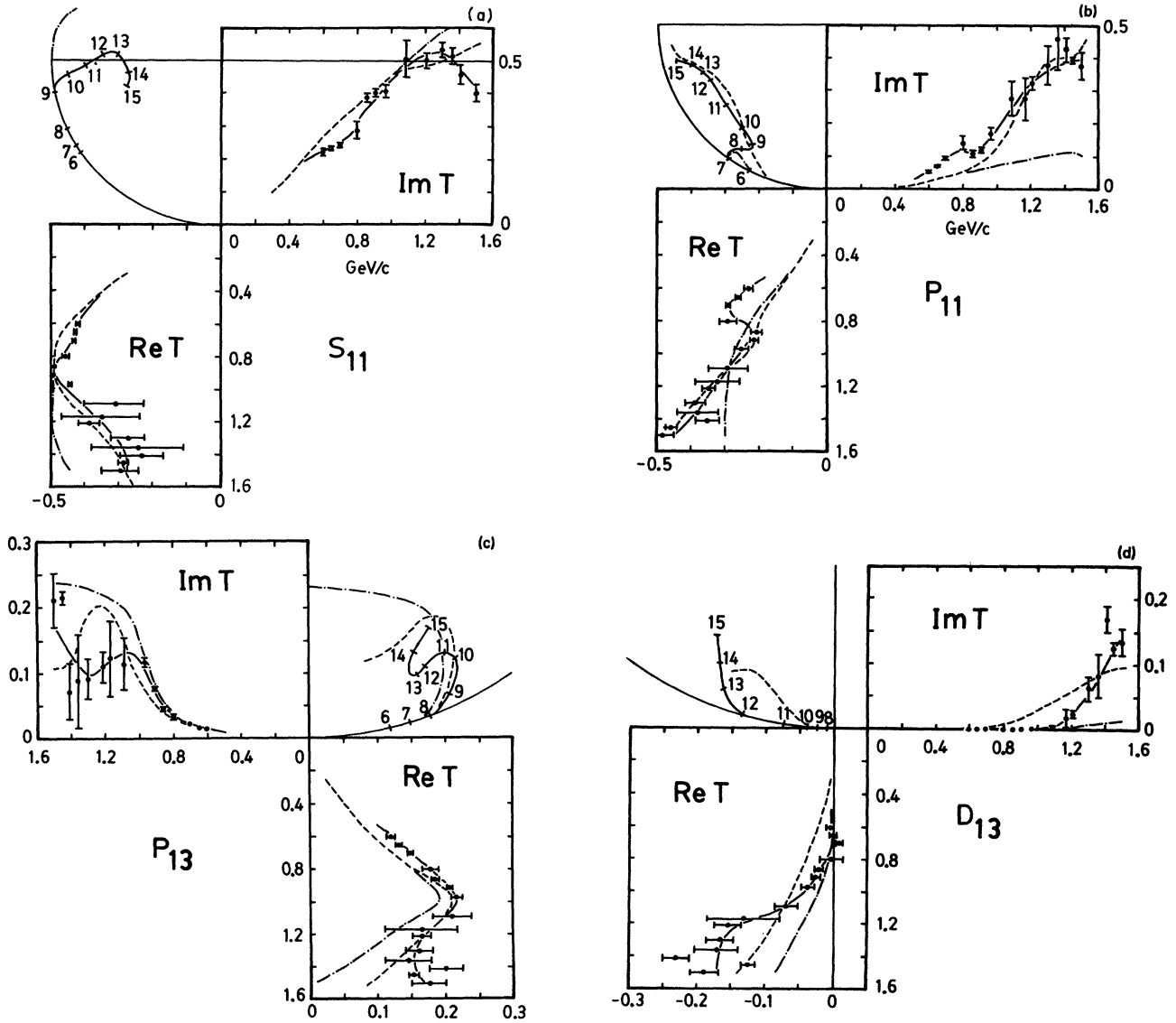

FIG. 4. The real and imaginary parts of KN partial waves and Argand diagrams. The real and imaginary parts are plotted versus P_{lab} in GeV/c. The dots with error bars are the present results, and the other solutions by Martin and Oades (Ref. 70) and by Nakajima *et al.* (Ref. 71) are plotted by dashed and dash-dotted curves, respectively. Solid curves are drawn by sight assuming smooth energy dependence of the real and imaginary parts of the present discrete solutions. Numbers in Argand diagrams are P_{lab} in 100 MeV/c.

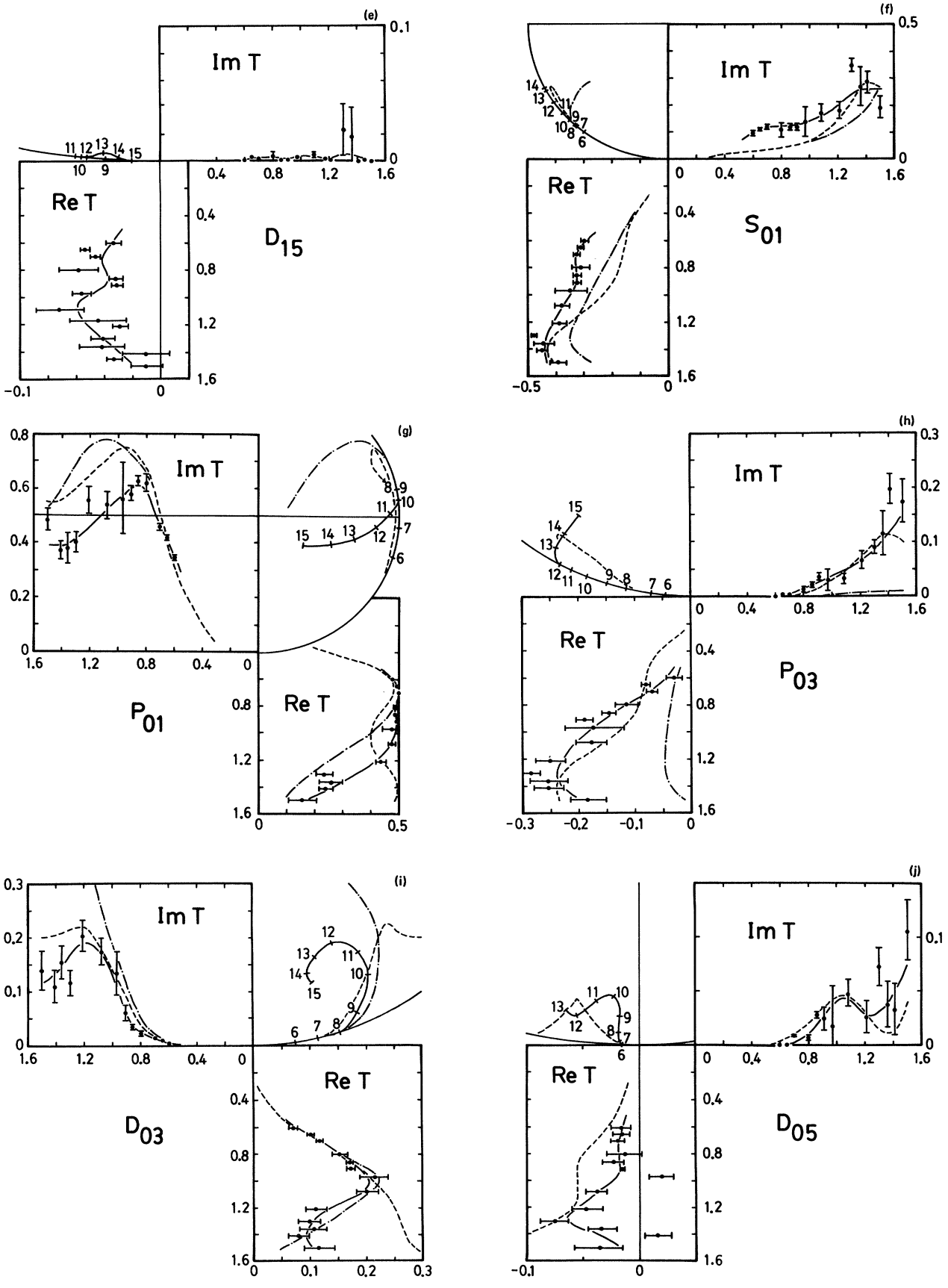

FIG. 4. (*Continued.*)

VI. DISCUSSIONS

As in Fig. 4 the present solution is consistent qualitatively with those by Martin and Oades[70] and Nakajima *et al.*[71] However, there are differences in many aspects.

In the $I=1$ system the P_{11} amplitude has a resonancelike structure between 700 and 900 MeV/c. This structure is overlooked in the other analyses. The behavior of P_{11} at around 900 MeV/c could be interpreted as a new candidate for Z_1^* resonances. The P_{13} wave, which has been interpreted as a Z_1^* resonance in some analyses,[73,74,61,71] also shows counterclockwise motion in the Argand diagram. We notice that the three solutions are consistent with each other for P_{13} up to 1000 MeV/c, but differ significantly in the appearance of absorption above 1000 MeV/c.

The contribution of the P waves to the K^+p total cross section is plotted in Fig. 6(a). We notice that the rapid rise of $\sigma_{tot}(K^+p)$ from 700 to 1200 MeV/c is clearly reflected in the peak of the P_{13} wave. The structure of P_{11} at around 900 MeV/c is not apparent in $\sigma_{tot}(K^+p)$.

The K^+p reaction cross section is plotted in Fig. 6(b) as well as the contribution from the P waves. Absorption in the K^+p channel occurs only above 600 MeV/c, and it is attributed solely to P_{11} up to 800 MeV/c. Since the P_{11} wave can be coupled to the $KN\pi$ channel through the P state of the $K\Delta$ channel, the resonance structure in P_{11} at 900 MeV/c is considered to have strong coupling to the $K\Delta$ channel.

In the $I=0$ system there is a large contribution from the P_{01} wave, which is very attractive even at low momenta. Some analyses in the KN $I=0$ state have claimed the possibility of a P_{01} resonance at around 900 MeV/c.[69,45,71] In the present analysis, however, it seems difficult to interpret the strong attractive nature of P_{01} as a simple Breit-Wigner resonance since no absorption is present up to 1000 MeV/c. At momenta higher than 1000 MeV/c, the P_{01} wave shows strong coupling to inelastic channels, most likely to K^*N, but the resonance structure is still unclear. On the contrary, the D_{03} wave shows typical behavior as a resonance. This is in contrast to the MO solution. A resonance in the D_{03} wave has been suggested by some analyses.[75,45,71] The present result reinforces the old D_{03} resonant solutions.

In Fig. 7(a) the contribution of P_{01} and D_{03} to the $I=0$ total cross section is plotted. The bump below 900 MeV/c is solely attributed to the large attractive P_{01}. The second bump at 1100 MeV/c is exactly the D_{03} resonance.

Figure 7(b) shows the partial wave contribution to the KN $I=0$ reaction cross section. Although the experimental data are not sufficient, the bump caused by the D_{03} resonance is apparent at 1100 to 1200 MeV/c. Since P_{01} is elastic up to 1000 MeV/c, there is no clear correspondence in σ_T ($I=0$).

Another structure can be seen in the D_{05} state. It shows inelasticity at low momenta around 700 MeV/c, which is even lower than the threshold of the K^*N channel. A similar tendency is also present in the MO solution. Although it is highly inelastic, a resonancelike loop is present in 800–1200 MeV/c. Concerning the fact that D_{05} can couple only to the K^*N D state, it seems difficult to understand the behavior of D_{05} without introducing a new dynamical effect.

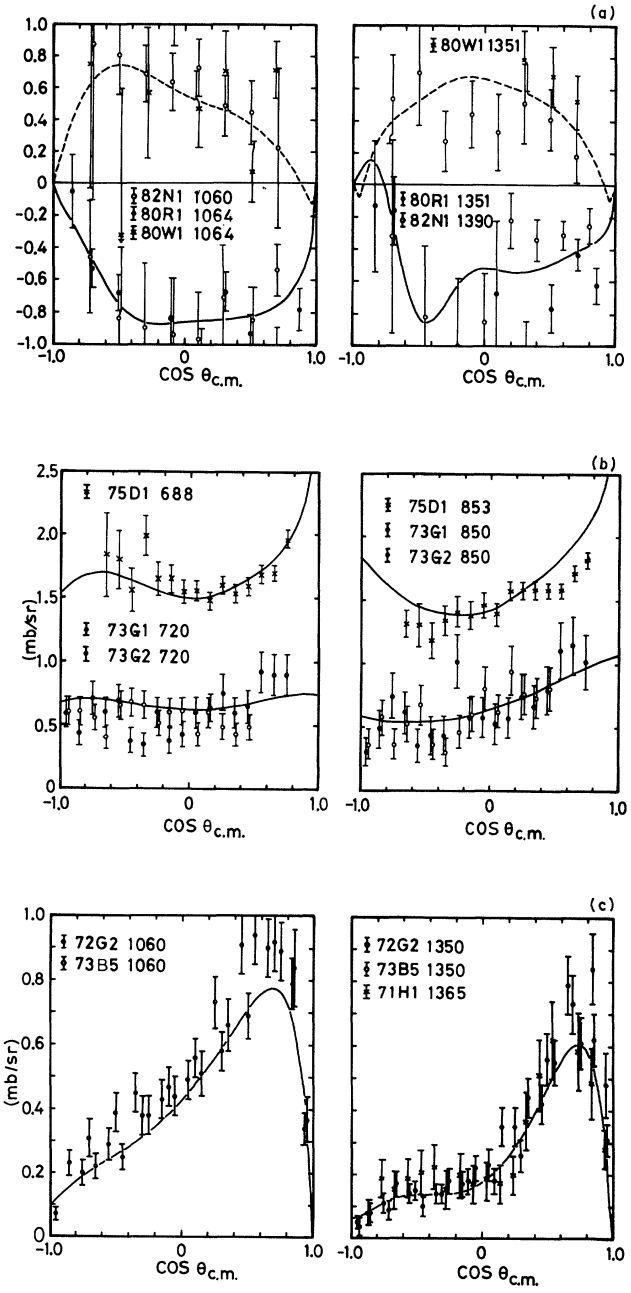

FIG. 5. (a) K^+n elastic and charge exchange polarizations at 1080 and 1360 MeV/c. The fit by the present solution is given by solid curves for $P(K^+n\to K^+n)$ and dashed curves for $P(K^+n\to K^0p)$. The data are from the Refs. 56–58. (b) cross sections for $K^+d\to K^+np$. Solid curves are calculated from the present results at 700 and 860 MeV/c including all three terms in Eq. (18) (upper) and neglecting I_n and J (lower). The calculation does not include the momentum cutoff for the individual experiments, nor the renormalization of the form factors. The experiment in Ref. 48 is for the events $K^+d\to K^+np$ or d, and the others are for $K^+d\to K^+n(p)$, where the proton is identified as the spectator by momentum cutoff. (c) Cross sections for $K^+d\to K^0pp$. Solid curves are calculated from the present results at 1080 and 1360 MeV/c. The data are from Refs. 51–53. The calculation does not include the momentum cutoff for the individual experiments, nor the renormalization of the form factors.

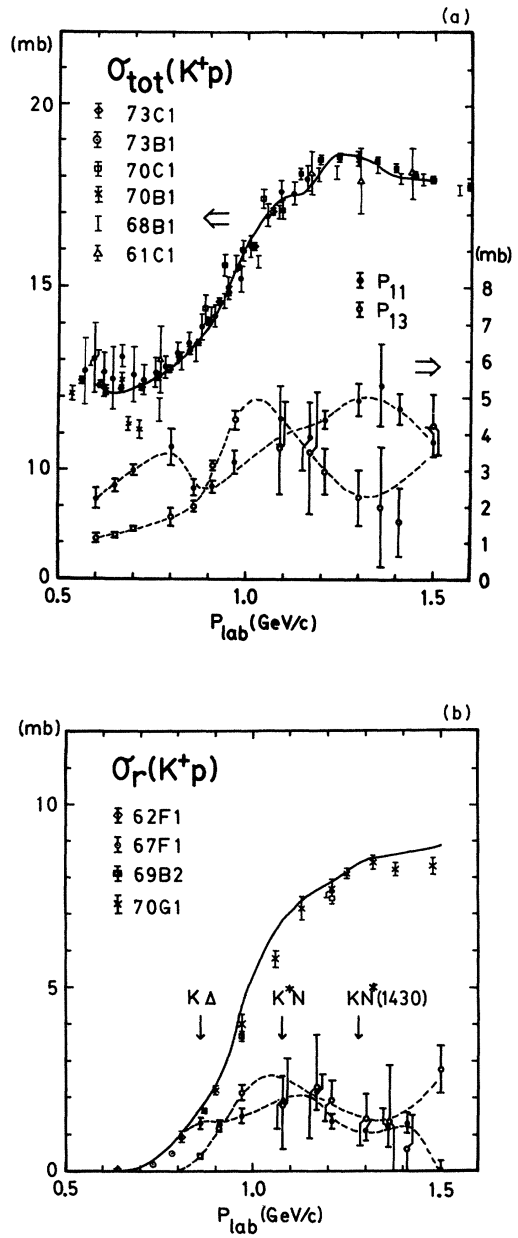

FIG. 6. Partial wave contributions to σ_{tot} (K^+p) and σ_r (K^+p). Solid curves are the fit to the data from Refs. 8 —14 and 16—18. Partial wave contributions are given by ● for P_{11} and ○ for P_{13} with error values. Dashed curves correspond to the continuous curves in Fig. 4.

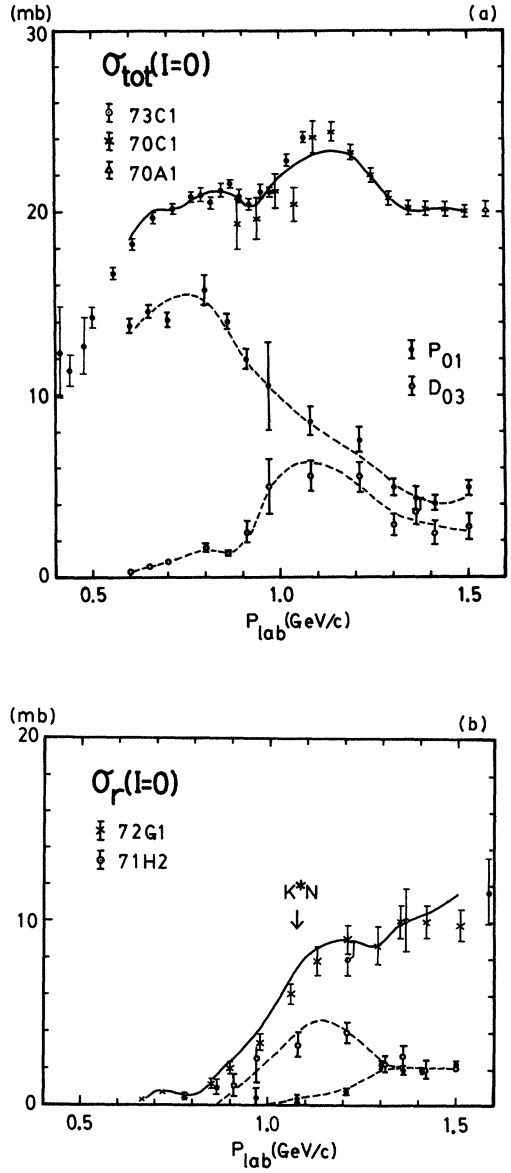

FIG. 7. Partial wave contributions to σ_{tot} ($I=0$) and σ_r ($I=0$). Solid curves are the fit to the data from Refs. 40—44. Partial wave contributions are given by ● for P_{01} and by ○ for D_{03} with error bars. Dashed curves correspond to the solid curves in Fig. 4.

We have discussed possible resonance states in Argand behavior. As in the other analyses, there is no resonance-like structure in the S waves for both the $I=1$ and $I=0$ states. Especially the S_{01} wave is elastic up to 1500 MeV/c in the present solution. In constituent quark models, the lowest $q^4\bar{q}$ states are considered in $J^P=\frac{1}{2}^-$. The MIT bag model[2] predicts such states in the KN $\frac{1}{2}^-$ state at around 800 MeV/c for $I=0$ and 1250 MeV/c for $I=1$.[4] In recent work by Jaffe and Low,[76] an appearance of multiquark states in scattering phenomena is discussed examining the concept of confinement, and it is shown that the conventional resonance picture does not necessarily hold for multiquark states. Using the P-matrix formalism developed there, analyses have been made to show such states are present in KN low partial waves as poles in the P matrix,[77,78] even though there is no structure in phase shifts. The absence of structures in the S waves may be explained as such. However, the structures in higher partial waves, shown in the present solution, seem to be consistent with the conventional picture of baryon resonances. At any rate, the present result will have to be examined in the light of the P-matrix formalism. The nu-

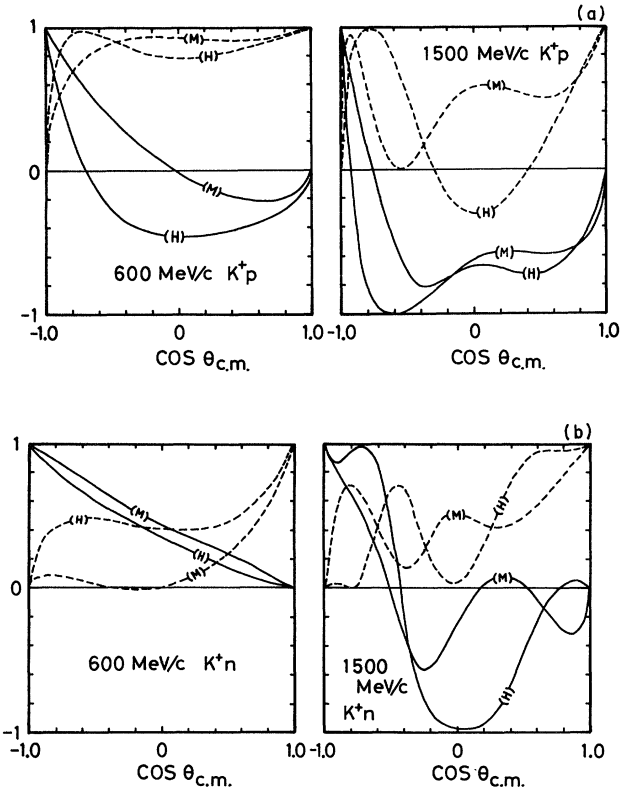

FIG. 8. Predictions for the R and A parameters at 600 and 1500 MeV/c for (a) K^+p and (b) K^+n elastic scattering. Solid curves are for the parameter R and dashed curves are for A. The predictions by the present solution and by the Martin-Oades solution (Ref. 70) are given with the marks (H) and (M) in the figure, respectively.

merical phase shifts listed in Table IV would provide a basis for such extended studies on exotic resonances.

It has sometimes been argued that the third angular observables independent of the differential cross section and the polarization are helpful in resolving ambiguities associated with amplitude analyses. Here we make predictions for the spin rotation parameters R and A. Their experimental definitions are schematically shown in Fig. 1, and the expressions are in Eq. (12). The prediction by the present solution and that by the MO solution are plotted in Fig. 8.

VII. CONCLUSIONS

The single energy scattering analysis has been presented for the KN $I=1$ and $I=0$ states at 600–1500 MeV/c. One motivation of the present work was due to the recent measurements of the polarization parameters for K^+n elastic and charge exchange scattering. The polarization data for the KN $I=0$ have not been available except for the single measurement at 600 MeV/c. As shown in Eq. (11), the polarization parameter can determine the relative phase of the spin amplitude, which is unavailable in the spin-averaged cross sections. Therefore, polarization data are necessary for reliable analyses, especially for a single energy analysis.

In analyzing the available data, special attention has been paid to the deuteron breakup reaction cross sections. The formalism is discussed in Sec. III, where it is emphasized that the spectator momentum cutoff creates a large normalization uncertainty for some breakup data. In fitting these data, it is necessary to introduce renormalization with comparable errors.

The obtained phase shifts are listed in Table IV with error values which reflect the quality of current experiments. Although the phase shifts are erroneous above 1000 MeV/c, we have found structures in some partial waves which have been overlooked in other analyses, probably owing to a particular parametrization or constraint used in those analyses. The result shows resonancelike loops in P_{11}, P_{13}, D_{03}, and D_{05}. In particular, the P_{13} and D_{03} waves, which have been candidates for Z^* resonances, have been found to show typical behavior as resonances at energies consistent with old resonant solutions. The loop in P_{11} at around 900 MeV/c has been found for the first time, which could be considered as a new candidate for Z_1^*. Even in the higher D_{05} wave, there is a highly inelastic resonancelike structure. This wave shows inelasticity at momenta even lower than the K^*N threshold, consistent with the analysis by Martin and Oades. Therefore, it seems to be difficult to explain the singular behavior of D_{05} as an effect due to the opening of known inelastic channels. The other candidate for Z_0^* resonances in the P_{01} state has not been clear in the present solution. The P_{01} wave is elastic up to 1000 MeV/c, and it seems difficult to interpret the strong attractive nature of P_{01} as a Breit-Wigner type of resonance.

The phase shifts listed in Table IV have been obtained in the model-independent analysis, free from any biases owing to a particular parametrization and constraint. These values will be used in calculations in kaon nuclear physics in the future. Also, they will provide a basis for extensive studies on exotic Z^* states like the P-matrix analysis.

ACKNOWLEDGMENTS

The author wishes to express his thanks to Dr. L. D. Roper and Dr. R. A. Arndt for valuable discussions and their hospitality at VPI&SU. The author is indebted to Dr. N. Hoshizaki for helpful suggestions. This work was supported by the United States Department of Energy, Contract No. DE-AS0576-ER04928.

[1]F. E. Close, *An Introduction to Quarks and Partons* (Academic, New York, 1979).
[2]A. Chodos, R. L. Jaffe, K. Johnson, C. B. Thorn, and V. F. Weisskopf, Phys. Rev. D 9, 3471 (1974).
[3]R. L. Jaffe, Phys. Rev. D 15, 267 (1977); 15, 281 (1977).
[4]D. Strottman, Phys. Rev. D 20, 748 (1979).
[5]C. B. Dover and G. E. Walker, Phys. Rep. 89, 1 (1982), and references therein.

[6]S. J. Watts *et al.*, Phys. Lett. 95B, 313 (1980); A. W. Robertson *et al.*, *ibid.* 91B, 465 (1980); K. Nakajima *et al.*, *ibid.* 112B, 75 (1982).
[7]K. Hashimoto, Prog. Theor. Phys. 66, 2300 (1981).
[8]V. Cook *et al.*, Phys. Rev. Lett. 7, 182 (1961) (61C1).
[9]D. V. Bugg *et al.*, Phys. Rev. 168, 1466 (1968) (68B1).
[10]R. L. Cool *et al.*, Phys. Rev. D 1, 1887 (1970) (70C1).
[11]T. Bowen *et al.*, Phys. Rev. D 2, 2599 (1970) (70B1).
[12]A. S. Carroll *et al.*, Phys. Lett. 45B, 531 (1973) (73C1).
[13]T. Bowen *et al.*, Phys. Rev. D 7, 22 (1973) (73B1).
[14]J. Fisk *et al.*, CERN report 1962, p. 358 (62F1).
[15]A. Bettini *et al.*, Phys. Lett. 16, 83 (1965).
[16]T. A. Filippas *et al.*, Nuovo Cimento 51A, 1053 (1967) (67F1).
[17]R. W. Bland *et al.*, Nucl. Phys. B13, 595 (1969) (69B2).
[18]G. Giacomelli *et al.*, Nucl. Phys. B20, 301 (1970) (70G1).
[19]S. C. Loken *et al.*, Phys. Rev. D 6, 2346 (1972).
[20]A. Berthon *et al.*, Nucl. Phys. B63, 54 (1973).
[21]T. F. Stubbs *et al.*, Phys. Rev. Lett. 7, 188 (1961).
[22]S. Goldhaber *et al.*, Phys. Rev. Lett. 9, 135 (1962).
[23]V. Cook *et al.*, Phys. Rev. 129, 2743 (1963).
[24]S. Focardi *et al.*, Phys. Lett. 24B, 314 (1967).
[25]A. S. Carroll *et al.*, Phys. Rev. Lett. 21, 1282 (1968).
[26]R. W. Bland *et al.*, Phys. Lett. 29B, 618 (1969).
[27]G. Giacomelli *et al.*, Nucl. Phys. B20, 301 (1970).
[28]P. K. Caldwell *et al.*, Phys. Rev. D 2, 1 (1970).
[29]M. G. Albrow *et al.*, Nucl. Phys. B30, 273 (1971).
[30]C. J. Adams *et al.*, Nucl. Phys. B66, 36 (1973).
[31]R. A. Burnstein *et al.*, Phys. Rev. D 10, 2767 (1974).
[32]W. Cameron *et al.*, Nucl. Phys. B78, 93 (1974).
[33]K. Abe *et al.*, Phys. Rev. D 11, 1719 (1975).
[34]B. J. Charles *et al.*, Nucl. Phys. B131, 7 (1977).
[35]M. G. Albrow *et al.*, Nucl. Phys. B30, 273 (1971).
[36]R. D. Ehrlich *et al.*, Phys. Rev. Lett. 26, 925 (1971).
[37]B. R. Barnett *et al.*, Phys. Rev. D 8, 2751 (1973).
[38]B. R. Lovett *et al.*, Phys. Rev. D 23, 1924 (1981).
[39]P. Baillon *et al.*, Nucl. Phys. B105, 365 (1976).
[40]R. L. Cool *et al.*, Phys. Rev. D 1, 1887 (1970) (70C1).
[41]R. J. Abrams *et al.*, Phys. Rev. D 1, 1917 (1970) (70A1).
[42]A. S. Carroll *et al.*, Phys. Lett. 45B, 531 (1973) (73C1).
[43]A. A. Hirata *et al.*, Nucl. Phys. B33, 525 (1971) (71H2).
[44]G. Giacomelli *et al.*, Nucl. Phys. B37, 577 (1972) (72G1).
[45]B. R. Martin, Nucl. Phys. B94, 413 (1975).
[46]G. Giacomelli *et al.*, Nucl. Phys. B56, 346 (1973).
[47]G. Giacomelli *et al.*, Istituto Nazionale di Fisica Nucleare Report INFN/AE-73/4, 1973 (unpublished).
[48]C. J. S. Damerell *et al.*, Nucl. Phys. B94, 374 (1975) (75D1).
[49]W. Slater *et al.*, Phys. Rev. Lett. 7, 378 (1961).
[50]A. K. Ray *et al.*, Phys. Rev. 183, 1183 (1969).
[51]A. A. Hirata *et al.*, Nucl. Phys. B30, 157 (1971) (71H1).
[52]G. Giacomelli *et al.*, Nucl. Phys. B42, 437 (1972) (72G2).
[53]P. Lugaresi-Serra *et al.*, Istituto Nazionale di Fisica Nucleare Report INFN/AE-73/9, 1973 (unpublished) (73B5).
[54]R. G. Glasser *et al.*, Phys. Rev. D 15, 1200 (1977).
[55]M. Sakitt, J. Skelly, and J. Thompson, Phys. Rev. D 15, 1846 (1977).
[56]A. W. Robertson *et al.*, Phys. Lett. 91B, 465 (1980) (80R1).
[57]K. Nakajima *et al.*, Phys. Lett. 112B, 75 (1982) (82N1).
[58]S. J. Watts *et al.*, Phys. Lett. 95B, 313 (1980) (80W1).
[59]R. M. Edelstein *et al.*, Phys. Rev. D 14, 702 (1976); J. C. M. Armitage *et al.*, Nucl. Phys. B123, 11 (1977).
[60]U. Casadei, G. Giacomelli, P. Lugaresi-Serra, G. Mandrioli, A. M. Rossi, and F. Viaggi, *A Compilation of K$^+$N Cross Sections Below 2 Gev/c,* CERN Report No. CERN/HERA 75-1, 1975.
[61]R. A. Arndt, L. D. Roper, and P. H. Steinberg, Phys. Rev. D 18, 3278 (1978).
[62]V. J. Stenger *et al.*, Phys. Rev. 134, B1111 (1964).
[63]G. Alberi *et al.*, Istituto Nazionale di Fisica Nucleare Report INFN/AE-72/3, 1972 (unpublished).
[64]L. Bertocchi and A. Capella, Nuovo Cimento 51A, 369 (1967).
[65]Alberi *et al.* (Ref. 63) employ the full three-body kinematics. Hence the off-shell nucleon mass appears in the calculation. Their formulas can be obtained by inserting the factor K in Eq. (21) in the integration. Stenger *et al.*, (Ref. 64) use a nonrelativistic phase space factor, so that the factor mE_q in Eq. (21) cancels with E_pE_q in the integrand of Eqs. (19) and (20).
[66]G. Giacomelli *et al.*, Nucl. Phys. 68B, 285 (1974); M. Sakitt *et al.*, Phys. Rev. D 12, 3386 (1975); R. G. Glasser *et al.*, *ibid.* 15, 1200 (1977).
[67]The Coulomb scattering effect is included only in the K$^+$p amplitude. This could be improved in the spirit of DWBA for the breakup reactions as in Stenger *et al.* (Ref. 23).
[68]T. Hamada and I. D. Johnston, Nucl. Phys. 34, 382 (1962); the employed parameters are from Humberston's revision. See C. Michael and C. Wilkin, Nucl. Phys. B11, 99 (1969).
[69]G. Giacomelli *et al.*, Nucl. Phys. B71, 138 (1974).
[70]B. R. Martin and G. C. Oades, in *Baryon 1980, Proceedings of the IVth International Conference on Baryon Resonances, Toronto,* edited by N. Isgur (University of Toronto Press, Toronto, 1981).
[71]K. Nakajima *et al.*, Phys. Lett. 112B, 80 (1982).
[72]The analysis at 1080 MeV/c is made at 1090 MeV/c for the $I=1$ state, while the $I=0$ state is analyzed at 1080 MeV/c with the $I=1$ amplitude fixed to the values at 1090 MeV/c.
[73]R. Ayed, P. Bareyre, J. Feltesse, and G. Villet, Phys. Lett. 32B, 404 (1970).
[74]S. Kato, P. Koehler, T. Novey, and A. Yokosawa, Phys. Rev. Lett. 24, 615 (1970).
[75]R. Aaron, M. Rich, W. L. Hogan, and Y. N. Srivastava, Phys. Rev. D 7, 1401 (1973).
[76]R. L. Jaffe and F. E. Low, Phys. Rev. D 19, 2105 (1979).
[77]C. Roiesnel, Phys. Rev. D 20, 1646 (1979).
[78]M. J. Corden *et al.*, Phys. Rev. D 25, 720 (1982).